Electron energy distribution in a dusty plasma: Analytical approach

I. B. Denysenko,[1,*] H. Kersten,[2] and N. A. Azarenkov[1]

[1]*School of Physics and Technology, V. N. Karazin Kharkiv National University, Svobody Square 4, 61022 Kharkiv, Ukraine*

[2]*Institut für Experimentelle und Angewandte Physik, Leibnizstrasse 19, Kiel D-24098, Germany*

(Received 30 June 2015; published 8 September 2015)

Analytical expressions describing the electron energy distribution function (EEDF) in a dusty plasma are obtained from the homogeneous Boltzmann equation for electrons. The expressions are derived neglecting electron-electron collisions, as well as transformation of high-energy electrons into low-energy electrons at inelastic electron-atom collisions. At large electron energies, the quasiclassical approach for calculation of the EEDF is applied. For the moderate energies, we account for inelastic electron-atom collisions in the dust-free case and both inelastic electron-atom and electron-dust collisions in the dusty plasma case. Using these analytical expressions and the balance equation for dust charging, the electron energy distribution function, the effective electron temperature, the dust charge, and the dust surface potential are obtained for different dust radii and densities, as well as for different electron densities and radio-frequency (rf) field amplitudes and frequencies. The dusty plasma parameters are compared with those calculated numerically by a finite-difference method taking into account electron-electron collisions and the transformation of high-energy electrons at inelastic electron-neutral collisions. It is shown that the analytical expressions can be used for calculation of the EEDF and dusty plasma parameters at typical experimental conditions, in particular, in the positive column of a direct-current glow discharge and in the case of an rf plasma maintained by an electric field with frequency $f = 13.56$ MHz.

DOI: 10.1103/PhysRevE.92.033102 PACS number(s): 52.25.Dg, 52.25.Vy, 52.27.Lw, 52.80.Pi

I. INTRODUCTION

Plasmas with nano- and micrometer-sized particles (dusty plasmas) have been extensively studied in the last three decades. These complex ionized gas systems are of great interest in different fields including formation of cosmic clouds, formation of Coulomb crystals, vortices, and voids in low-pressure plasmas, as well as in the fields of fusion and processing plasmas [1–5].

Because of the fundamental and technological interest, properties of dusty plasmas have been studied by many authors and are quite well known [1–7]. They include the balance of electrons and ions, charging of dust particles, structure formation, wave and shock propagation in the plasmas, transport of electrons, ions, and dust particles, and forces affecting the dust particles [1–4,8–14].

For a theoretical description of these complex systems, one usually uses hydrodynamic models for the electrons and ions assuming that they are in Maxwellian equilibrium [1–4,9]. However, for most industrial and laboratory plasmas such as those from inductively and capacitively coupled discharges, the electron energy distribution function (EEDF) often deviates from Maxwellian because of the many different electron collision processes [15,16]. The profile of the electron energy distribution function affects different plasma parameters such as the effective electron temperature, the electron and ion number densities, and the reaction rate coefficients, as well as the dust charge and the ion and/or electron fluxes on a processing surface [1,17,18]. Moreover, the collective motion of dusty plasma, for example, the propagation of vertically polarized dust acoustic waves, also depends on the EEDF profile [19]. Therefore, determination of the EEDF profile is very important in studying different plasmas.

In [20], the electron energy probability function in a dusty plasma was analyzed from the second derivative of the Langmuir probe current-voltage characteristics. It was found that in the presence of dust particles the electron density decreased and the electron temperature increased in comparison to those of pristine argon plasma [20]. The population of lower-energy electrons decreased in a dusty plasma, while the high-energy tail region overlapped throughout the experiment. In [21], optical emission spectroscopy was performed on a radio-frequency (rf) discharge in argon during dust particle growth. It was found that the intensities of all of the argon emission lines increased due to increasing electron temperature, indicating an increase in the number of high-energy electrons in the EEDF as a result of dust growth. The increase of emission intensity from plasmas with increasing dust size was also observed in [22,23].

In [24], the EEDF for a magnetically filtered dusty plasma was studied in a dusty double plasma device. In the experiment, it was observed that typical Druyvesteyn-like EEDFs in pristine plasma may behave as Maxwellian types in the presence of a sufficient concentration of dust grains, as was predicted before in [25]. In [26], an image of the electron temperature in a dusty plasma was observed. It was found that the electron temperature was lower in the void region than in the surrounding plasma region with dust particles. Later, by solving the electron Boltzmann equation, the electron temperature increase in the dusty region was explained by the fact that the rf electric field is inversely proportional to the local electron density [27].

For calculation of the EEDF in dusty plasmas, different numerical approaches have been used. To study dusty plasma properties, McCaughey and Kushner [28] developed a hybrid Monte Carlo–molecular dynamics approach, while Boeuf

*Corresponding author: idenysenko@yahoo.com

[29] introduced a particle-in-cell–Monte Carlo (PIC-MC) model. Numerical models for reactive rf dusty plasmas were developed by Schweigert *et al.* [30] and Goedheer *et al.* [31]. In [32], a method for calculation of dust charging in a capacitively coupled rf discharge was developed based on the kinetic treatment of the electron and ion motion using the PIC-MC approach. It was shown that at large ion drift velocities, the orbital-motion-limited (OML) theory gives up to 25% larger absolute value of the dust potential than that obtained with the PIC-MC calculations. Self-consistent kinetic models of low-pressure glow discharges with dust particles based on the Boltzmann equation for the electron energy distribution function were presented in [33]. In [34], nonlocal effects in the positive column (PC) of a low-pressure stratified dc glow discharge in argon with dust particles were studied. It was noted that in a stratified PC the electron energy distribution is not Maxwellian and is even nonmonotonic, and the local field approximation is appropriate for the EEDF calculation only at intermediate gas pressures. The EEDF in a dusty plasma was obtained on the basis of the solution of the homogeneous Boltzmann equation by Wang and Dong [35]. Considering the case when an external electric field sustaining a dusty plasma is fixed, they found that the profile of the EEDF strongly depends on the dust concentration. rf discharges with dust were investigated with the help of the homogeneous Boltzmann equation for the EEDF in [25,27,36–38], too. However, all these numerical approaches for determination of the EEDF in dusty plasmas are rather complicated. Suitable analytical expressions for the EEDF in dusty plasmas, accounting for deviations of the distribution from Maxwellian, are not available at present.

Meantime, for dust-free plasmas, different analytical expressions for the EEDF were obtained in some cases, by applying the two-term approximation [17,39–41]. In particular, using this approximation, the Druyvesteyn distribution function, describing the steady-state electron distribution function in a uniform plasma and with elastic collisions between electrons and neutral gas atoms, was obtained [17,40]. In this approach, an analytical expression was also derived for the EEDF in a positive column for electrons with energies exceeding the first inelastic energy threshold $U_{\rm exc}$ [17,40,41].

In this paper, we will provide an analytical expression for the EEDF in an argon dusty plasma for electrons with energies exceeding $U_{\rm exc}$. We will also derive an integral expression for the electron energy distribution function for electrons in the energy range smaller than $U_{\rm exc}$. We will show that the analytical expressions can be used for calculation of the EEDF in rf and dc dusty plasmas. These analytical expressions for the EEDF will be obtained in the local approximation [17] neglecting electron-electron collisions and neglecting transformation of high-energy electrons into low-energy electrons at inelastic electron-atom collisions. The electron energy distribution function, the effective electron temperature, and the dust charge obtained from the simplified model will be compared with those calculated numerically using a more complicated approach, in which electron-electron collisions and the transformation of high-energy electrons at inelastic electron-neutral collisions are not neglected. The study is carried out for different dust radii and densities, as well as for different frequencies, electron densities, and rf field amplitudes. Typical conditions, where the simplified approach for EEDF determination in dusty plasmas is applicable, will be reported.

II. MAIN ASSUMPTIONS AND EQUATIONS

Let us consider a plasma maintained by an electric field $E(t)$. In the case of a radio-frequency discharge $E(t) = E_p \cos(\omega t)$, where $\omega = 2\pi f_E$ and f_E is the rf frequency. For a direct current discharge, $E(t) = E_p = \text{const}$. The plasma is assumed to consist of electrons with density n_e, singly charged positive ions (Ar^+) with density n_i, and negatively charged dust particles of submicron size with density n_d and radius a_d. We also assume that the dust grains are all of the same size and are uniformly distributed in the plasma volume. The massive dust grains (as compared with the ions and electrons) can be treated as immobile, when $\tau_d \gg \tau_{\rm eq}$, where τ_d and $\tau_{\rm eq}$ are the characteristic time scales of dust grain motion and establishment of equilibrium, respectively. It is also assumed that the dust radius is smaller than the sheath around a dust grain, or $\lambda_D \gg a_d$, where $\lambda_D \approx 1/\sqrt{4\pi e(n_e/T_{\rm eff} + n_i/T_i)}$ is the Debye length, and e is the magnitude of electron charge, $T_{\rm eff}$ (in eV) is the effective electron temperature, and T_i (in eV) is the ion temperature. The effective electron temperature is defined by the electron energy distribution function $f_0(u)$: $T_{\rm eff} = (2/3)\int_0^\infty f_0(u)u^{3/2}du$, where u is the electron energy (in eV) and $f_0(u)\sqrt{u}du$ is the ratio of the number of electrons with energy in the interval $[u,u+du]$ to the total number of electrons.

The distance between the dust particles is larger than the Debye length. We consider dust particles of small radius ($a_d < 1\,\mu$m) and, therefore, the linear Debye-Hückel potential can be taken as the shielding potential of the dust grain [1],

$$\varphi(r) = \varphi_s \frac{a_d}{r} \exp\left[-(r-a_d)/\lambda_D\right],$$

where r is the distance from the dust particle center, and ϕ_s is the grain surface potential.

To calculate the electron energy distribution function, the two-term approximation is used, whereas the energy distribution is assumed to be nearly isotropic. This assumption is valid if the electron dynamics is dominated by elastic collisions over most of the energy range, i.e., the elastic scattering frequency of electrons must be large compared to the characteristic frequencies for electron energy gain (e.g., from the field) and loss (e.g., due to inelastic collisions) [17].

For the rf case, it is assumed that the field variation is much faster than that of energy relaxation, or $\omega > \nu_e = (2m_e/m_i)\langle\nu_{em}\rangle + \langle\nu^*\rangle$, where m_e and m_i are the masses of electrons and ions, respectively. ν_{em} is the rate of electron-neutral momentum transfer, ν^* is the total inelastic collision frequency, and $\langle\cdots\rangle$ denotes the energy-averaged value. Thus, in both the rf and dc cases, the isotropic part of the electron energy distribution function can be treated as time independent [42,43].

Moreover, we assume that the energy relaxation length λ_ε is small compared to the spatial inhomogeneity scale Λ of the discharge,

$$\lambda_\varepsilon \ll \Lambda, \tag{1}$$

where $\lambda_\varepsilon \approx (\lambda_m \lambda_{\rm inel}/3)^{1/2}$ [17]. Here, $\lambda_m \approx 1/(n_a\langle\sigma_m\rangle + n_d\langle\sigma_{ed}\rangle)$ is the total mean free path for momentum transfer, and $\lambda_{\rm inel}$ is the mean free path accounting for all collisional loss processes. The mean free path can be estimated as

$$\lambda_{\rm inel}^{-1} \approx n_a[(2m_e/m_i)\langle\sigma_m\rangle + \langle\sigma_{ex}\rangle + \langle\sigma_{iz}\rangle] + n_d\big[(2m_e/m_d)\big\langle\sigma_{ed}^e\big\rangle + \big\langle\sigma_{ed}^c\big\rangle\big],$$

where n_a is the neutral gas density, σ_m is the cross section for electron-atom momentum transfer collisions, σ_{ex} is the total cross section for electronic excitation in collisions of electrons with Ar atoms, σ_{iz} is the cross section for electron impact ionization in collisions of electrons with Ar atoms, and m_d is the individual dust particle mass. σ_{ed}^e and σ_{ed}^c are the cross sections for momentum transfer collisions of electrons with dust particles and collection of electrons by dust particles, respectively. In a plasma with large dust density, the condition (1) takes place at smaller gas pressures than in the dust-free plasma [36]. In this case, one can use the local approximation, and the electron energy distribution function can be presented in the form $F_0 = n_e f_0(u)$. The function f_0 is normalized by $\int_0^\infty f_0(u)\sqrt{u}du = 1$.

The electron energy distribution function f_0 satisfies the following homogeneous Boltzmann equation [39,40]:

$$-\frac{2e}{3m_e}\frac{\partial}{\partial u}\left[\frac{u^{3/2}}{\nu_m(u)}E_{\rm eff}^2(u)\frac{\partial f_0}{\partial u}\right] = S_0(f_0), \tag{2}$$

where

$$E_{\rm eff}^2 = \frac{E_{\rm p}^2}{2}\frac{\nu_m^2(u)}{\nu_m^2(u)+\omega^2}$$

for the rf case, and $E_{\rm eff} = E_p$ is the external electric field in the dc case. Here, $S_0(f_0) = S_{ea}(f_0) + S_{ed}(f_0) + S_{ee}(f_0)$, where the terms $S_{ea}(f_0)$, $S_{ed}(f_0)$, and $S_{ee}(f_0)$ describe the electron-atom, electron-dust, and electron-electron collisions, respectively. ν_m is the effective rate of momentum transfer, including electron-neutral and electron-dust collisions. In this approximation superelastic collisions between electrons and atoms, as well as excitation from low to high atomic states, are neglected.

The term describing electron-atom collisions has several components. The elastic collisions are represented by

$$S_{ea}^e(f_0) = \frac{d}{du}\left[\frac{2m_e}{m_i}u^{3/2}\nu_{em}(u)\left(f_0 + T_g\frac{df_0}{du}\right)\right], \tag{3}$$

where T_g is the neutral gas temperature, which is assumed to be equal to 300 K (0.026 eV). The collision-induced atomic excitations are given by

$$S_{ea}^{\rm exc}(f_0) = \sum_k \big\lfloor \nu_{ea}^k(u+V_k)f_0(u+V_k)(u+V_k)^{1/2} - \nu_{ea}^k(u)f_0(u)u^{1/2}\big\rfloor, \tag{4}$$

where ν_{ea}^k is the collision frequency of the kth inelastic process with a threshold energy V_k. In this model the ionization of Ar atoms is treated as an ordinary excitation process [44]. The term describing electron-dust collisions can be modeled by [35]

$$S_{ed}(f_0) = \frac{d}{du}\left[\frac{2m_e}{m_d}u^{3/2}\nu_{ed}^e(u)\left(f_0 + T_d\frac{df_0}{du}\right)\right] - \nu_{ed}^c(u)f_0u^{1/2}, \tag{5}$$

where T_d is the individual dust particle temperature. It is assumed that $T_d = 0.026\,{\rm eV}$ and $m_d = (4/3)\rho_d\pi a_d^3$, where $\rho_d = 2g/{\rm cm}^3$ is the dust material density [1]. $\nu_{ed}^e(u) = n_d\sigma_{ed}^e(u)(2eu/m_e)^{0.5}$ and $\nu_{ed}^c(u) = n_d\sigma_{ed}^c(u)(2eu/m_e)^{0.5}$ are the frequencies for electron-dust momentum transfer and electron collection by the dust particles, respectively. The cross section for electron-dust momentum transfer is [35]

$$\sigma_{ed}^e(u) \approx \pi a_d^2(-\varphi_s/u)^2 e^{2a_d/\lambda_D}\ln\chi, \tag{6}$$

where $\chi \approx -\lambda_D T_{\rm eff}/(a_d\varphi_s)$. In the orbital-motion-limited approximation the cross section for collection of electrons by the dust particles is $\sigma_{ed}^c(u) = \pi a_d^2(1+\varphi_s/u)$ for $u \geqslant -\varphi_s$ and $\sigma_{ed}^c(u) = 0$ for $u < -\varphi_s$.

The term $S_{ee}(f_0)$ describing electron-electron collisions is given by

$$S_{ee}(f_0) = \frac{d}{du}\left[2u^{3/2}\nu_{ee}(u)\left(f_0G(u) + H(u)\frac{df_0}{du}\right)\right], \tag{7}$$

where $H(u) = \frac{2}{3}(\int_0^u u^{3/2}f_0(u)du + u^{3/2}\int_u^\infty f_0(u)du)$, $G(u) = \int_0^u u^{1/2}f_0(u)du$, $\nu_{ee}(u) = 4\pi(e^2/m_e)^2 n_e\ln\Lambda/\upsilon^3$, $\ln\Lambda$ is the Coulomb logarithm [40], and $\upsilon = \sqrt{2eu/m_e}$ is the electron velocity.

It is assumed that the electron (I_e) and ion (I_i) currents to a floating dust particle are in balance, or

$$I_e + I_i = 0. \tag{8}$$

The electron current to a dust particle is [45]

$$I_e = -\pi a_d^2 e n_e\int_{-\varphi_s}^\infty\left(1+\frac{\varphi_s}{u}\right)\sqrt{\frac{2eu}{m_e}}f_0(u)\sqrt{u}du.$$

The ion current was calculated taking into account the ion-neutral collisions in the sheath around a dust particle, resulting in [46]

$$I_i = en_i a_d^2(8\pi T_i/m_i)^{0.5}(1+\xi\tau + H\xi^2\tau^2\lambda_S n_a\sigma_{ia}),$$

where $\tau = T_{\rm eff}/T_i$ and $\xi = |Z_d|e^2/(a_d T_{\rm eff})$, and $\sigma_{ia} \approx 10^{-14}\,{\rm cm}^{-2}$ is the cross section for ion-neutral collisions. We assume that $T_i = T_g$. The function H has the following asymptotes: $H \sim 0.1$ for $0.1 \leqslant \beta \leqslant 10$; $H \sim \beta$ for $\beta \ll 1$, and $H \sim \beta^{-2}(\ln\beta)^3$ for $\beta \gg 1$ [46], where $\beta = |Z_d|e^2/(\lambda_s T_i)$ and λ_s is the screening length, which is of the same order as the Debye length [1].

Furthermore, it is assumed that the plasma is quasineutral, or

$$n_i = n_e + |Z_d|n_d. \tag{9}$$

Equations (8) and (9) are used to calculate the dust charge required for the term (5) describing electron-dust collisions.

In general, the EEDF from Eq. (2) may be found only numerically. However, as shown below, an approximate analytical solution of Eq. (2) also exists.

III. THE APPROXIMATE ANALYTICAL SOLUTION FOR THE EEDF

Consider the case of low-ionized plasma [the electron-atom collisions dominate over the electron-electron collisions, i.e., $\nu_{ee}/(\delta\nu_{em}) \ll 1$ for most of the electrons' energies in the electron energy distribution, where $\delta = 2m_e/m_i$]. Moreover, the number of electrons with energy larger than the first excitation energy threshold ($\approx$11.5 eV for Ar) is assumed to be small. In this case, one can neglect in Eq. (2) the term (7) and the term describing transformation of electrons with large energy into low-energetic electrons, and Eq. (4) can be simplified to

$$S_{ea}^{\mathrm{exc}}(f_0) \approx -\sum_k \nu_{ea}^k(u) f_0(u) u^{1/2}. \tag{10}$$

Taking into account these simplifications, the homogeneous Boltzmann equation can be written as

$$\frac{\partial}{\partial u}\left[u^{3/2}\left(\delta_D \nu_{ed}^e(u) + \delta\nu_{em}(u)\right)\left\{f_0(u) + \frac{1}{\beta}\frac{\partial f_0(u)}{\partial u}\right\}\right] \approx \left[\nu_{ed}^c(u) + \nu_{1\Sigma}(u)\right] f_0(u)\sqrt{u}, \tag{11}$$

where $\delta_D = 2m_e/m_d$,

$$\beta^{-1} = T_g + \frac{2e}{3m_e}\frac{E_{\mathrm{eff}}^2}{\nu_m(\delta_D\nu_{ed}^e + \delta\nu_{em})},$$

$\nu_m = \nu_{ed}^e + \nu_{em}$, and $\nu_{1\Sigma}(u) = \sum_k \nu_{ea}^k(u)$ is the total frequency for inelastic electron-atom collisions including processes of excitation and ionization. The frequency was calculated using Eqs. (B6) and (B7) of Ref. [47].

At large electron energies ($u \geqslant u_1^* > u^* = 11.5$ eV, and by taking $u_1^* = 20$ eV), the electron energy distribution function decreases rapidly with an increase of u. Therefore, to calculate the EEDF at large energies, we apply the quasiclassical method [17,40,41] assuming that

$$f_0(u) = C_2 \exp[S(u)], \tag{12}$$

where C_2 is a constant, and $S(u)$ is a smooth function satisfying the following conditions [40]:

$$u\frac{dS}{du} \gg 1 \text{ and } \left(\frac{dS}{du}\right)^2 \gg \left|\frac{d^2S}{du^2}\right|.$$

In this approximation, it follows from Eq. (11) that

$$\frac{dS(u)}{du} = -\frac{1}{\sqrt{u}}\sqrt{\frac{\beta\left[\nu_{ed}^c(u) + \nu_{1\Sigma}(u)\right]}{\delta_D\nu_{ed}^e(u) + \delta\nu_{em}(u)}} = -\beta_1(u)$$

and

$$S(u) = -\int_{u_1^*}^{u} \beta_1(u')du'. \tag{13}$$

At large electron energies (e.g., $\delta_D\nu_{ed}^e \ll \delta\nu_{em}$ and $\nu_{ed}^e \ll \nu_{em}$) and, therefore, the ratio of β_1 in a dusty plasma to that in a dust-free plasma for the same electric field sustaining the plasmas is approximately $\sqrt{[\nu_{ed}^c(u) + \nu_{1\Sigma}(u)]/\nu_{1\Sigma}(u)}$. Thus, at large electron energies the EEDF in a dusty plasma decreases faster than in a dust-free plasma.

In the pristine case when $n_d = 0$, it follows from (13) that [40,41]

$$S(u) = -\int_{u_1^*}^{u}\sqrt{\frac{3m_e\nu_{em}(u')\nu_{1\Sigma}(u')}{u'2eE_{\mathrm{eff}}^2}}du'.$$

To calculate the EEDF at moderate and low energies ($u < u_1^*$), we move from u to the new variable $y = u_1^* - u$. In this case, Eq. (11) can be presented in the following form:

$$-\frac{\partial}{\partial y}\left[\alpha(y)\left\{f_0(y) - \frac{1}{\beta}\frac{\partial f_0(y)}{\partial y}\right\}\right] \approx \left[\nu_{ed}^c(y) + \nu_{1\Sigma}(y)\right] f_0(y)\sqrt{u_1^* - y}, \tag{14}$$

where $\alpha(y) = u^{3/2}[\delta_D\nu_{ed}^e(u) + \delta\nu_{em}(u)]$ with $u = u_1^* - y$.

Integrating Eq. (14) in the energy interval $[0, y]$, we obtain

$$-\alpha(y)\left\{f_0(y) - \frac{1}{\beta}\frac{\partial f_0(y)}{\partial y}\right\} + A \approx \int_0^y \left[\nu_{ed}^c(y') + \nu_{1\Sigma}(y')\right] f_0(y')\sqrt{u_1^* - y'}dy', \tag{15}$$

where

$$A = \alpha(y)\left\{f_0(y) - \frac{1}{\beta}\frac{\partial f_0(y)}{\partial y}\right\}\Big|_{y=0}.$$

We assume that $f_0(y=0) = C_2$. Therefore, it follows from Eqs. (12) and (13) that $\frac{\partial f_0(y)}{\partial y}|_{y=0} = C_2\beta_1(y=0)$.

Equation (15) may be presented in the following form:

$$f_0(y) - \frac{1}{\beta}\frac{\partial f_0(y)}{\partial y} = \chi(y), \tag{16}$$

where

$$\chi(y) = \frac{A - \int_0^y \left[\nu_{ed}^c(y') + \nu_{1\Sigma}(y')\right] f_0(y')\sqrt{u_1^* - y'}dy'}{\alpha(y)}.$$

The solution of Eq. (16) is

$$f_0(y) = \left[C_2 - \int_0^y \beta(y')\chi(y')\exp\left(-\int_0^{y'}\beta(y'')dy''\right)dy'\right] \times \exp\left(\int_0^y \beta(y')dy'\right). \tag{17}$$

Note that the integral expression for $\chi(y)$ depends on the EEDF. However, it can be easily calculated because the energy distribution function at $y = 0$ is known [$f_0(y=0) = C_2$]. As a result,

$$I_1 = \int_0^{\Delta y}\left[\nu_{ed}^c(y) + \nu_{1\Sigma}(y)\right] f_0(y)\sqrt{u_1^* - y}dy \approx \left[\nu_{ed}^c(y=0) + \nu_{1\Sigma}(y=0)\right] f_0(y=0)\sqrt{u_1^*}\Delta y,$$

where $\Delta y \ll u_1^*$, and one can find from Eq. (17) the EEDF at $y = \Delta y$. Similarly, one can calculate the integral for $y = 2\Delta y$ to be $I_2 = \int_0^{2\Delta y}[\nu_{ed}^c(y) + \nu_{1\Sigma}(y)]f_0(y)\sqrt{u_1^* - y}dy \approx I_1 + [\nu_{ed}^c(y=\Delta y) + \nu_{1\Sigma}(y=\Delta y)]f_0(y=\Delta y)\sqrt{u_1^* - \Delta y}\Delta y$, and then one can find f_0 at $y = 2\Delta y$. After getting f_0 at $y = 2\Delta y$, one can obtain the EEDF at $y = 3\Delta y$, etc. Thus, Eqs. (12) and (17) allow us to obtain the EEDF in the whole energy interval. The constant C_2 in Eqs. (12)

and (17) was found from the normalization condition $[\int_0^\infty f_0(u)\sqrt{u}du = 1]$.

IV. RESULTS

In this section, we will analyze how the electron energy distribution function depends on the dust density and the dust particle radius, and we will determine the range of parameters where the simplified approach may be applied. To analyze the applicability of the simplified model, we will compare the EEDF obtained from Eqs. (12) and (17) with that calculated from Eq. (2) using a finite-difference method [25] for different rf frequencies, electron densities, and rf field amplitudes.

A. The effect of dust particles on the EEDF and other dusty plasma properties

First, we study how the variations of dust density and dust radius affect the electron energy distribution function. In Fig. 1(a), the EEDF is shown for dust densities $n_d = 3 \times 10^7$ cm^{-3}, $n_d = 5 \times 10^7$ cm^{-3}, and $n_d = 10^8$ cm^{-3}, as well as for the case when dust particles in the rf discharge are absent ($n_d = 0$). The curves in Fig. 1(a) were obtained using the simplified model for the following rf discharge parameters: $f = 13.56$ MHz, $p = 13.3$ Pa, $T_g = 300$ K, $n_e = 10^9$ cm^{-3}, $a_d = 200$ nm, and $E_p = 300$ V/m. One can see from Fig. 1(a) that for the same external electric field sustaining the plasma, the number of electrons with energies larger than 6 eV is smaller in the dusty plasma than in the dust-free plasma.

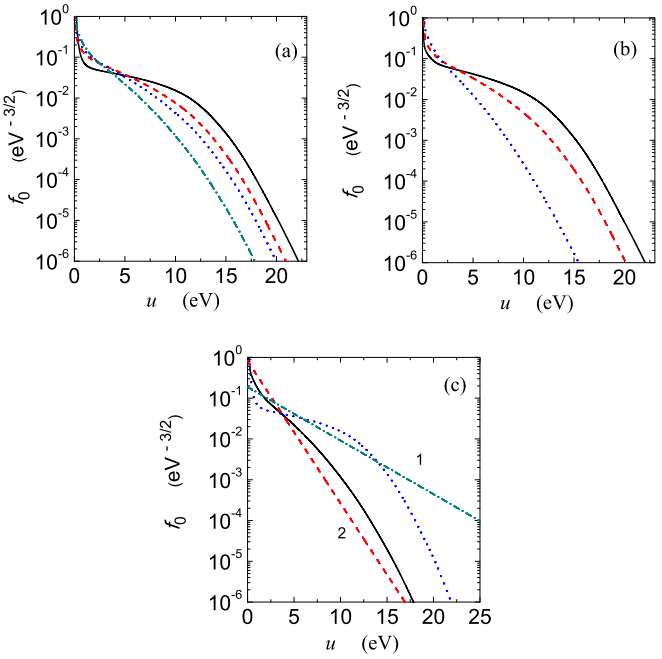

FIG. 1. (Color online) (a) The electron energy distribution function calculated using the simplified model for $a_d = 200$ nm and different dust densities: $n_d = 0$ (solid line), 3×10^7 cm^{-3} (dashed line), 5×10^7 cm^{-3} (dotted line), and $= 10^8$ cm^{-3} (dash-dotted line). (b) The same as in (a) for $n_d = 3 \times 10^7$ cm^{-3} and different dust radii: $a_d = 100$ nm (solid line), $a_d = 250$ nm (dashed line), and $a_d = 500$ nm (dotted line). (c) The EEDF calculated using the simplified model for $n_d = 0$ (dotted line) and 10^8 cm^{-3} (solid line). The Maxwellian EEDF calculated at $T_{\rm eff} = 3.30$ eV corresponding to $n_d = 0$ (curve 1) and at $T_{\rm eff} = 1.24$ eV corresponding to $n_d = 10^8$ cm^{-3} (curve 2). The other external conditions are the same as in (a).

TABLE I. The dust charge, effective electron temperature, and dust surface potential for different dust densities and dust radii. The external conditions correspond to Fig. 1.

n_d (10^7 cm^{-3})	a_d (nm)	$Z_d(-e)$	$T_{\rm eff}$ (eV)	φ_s (V)
0	200	736	3.30	5.30
0.5	200	553	3.64	3.98
2	200	366	2.83	2.64
3	200	308	2.45	2.22
5	200	238	1.92	1.71
10	200	154	1.24	1.11
3	100	214	3.40	3.08
3	250	329	1.98	1.90
3	500	359	0.82	1.03

The number of energetic electrons is decreasing with increasing dust density. The decrease is due to the increase of the total surface of dust particles absorbing the electrons with energy u larger than the dust surface potential φ_s. The decrease of energetic electron's number is accompanied by

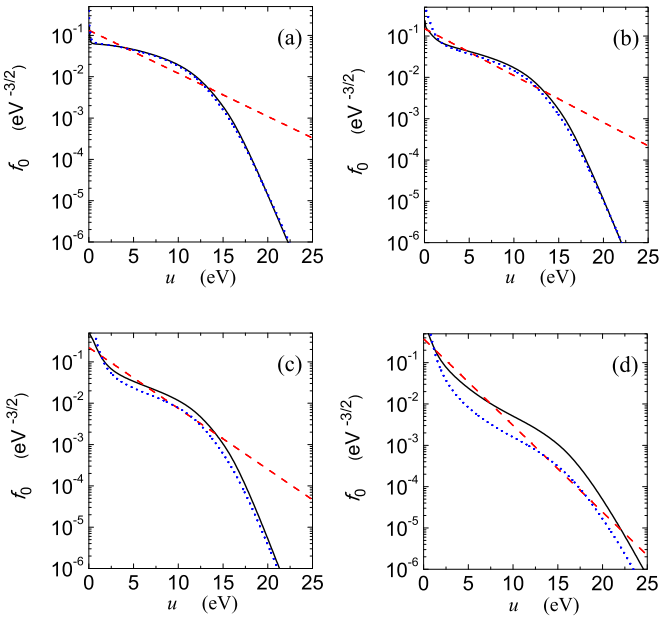

FIG. 2. (Color online) EEDFs calculated using the more complicated numerical (solid lines) and simplified analytical (dotted lines) models for $n_d = 10^7$ cm^{-3}, $a_d = 100$ nm, and different rf frequencies: 0 (a), 27.12 MHz (b), 60 MHz (c), and 2.45 GHz (d). $E_p = 8500$ V/m for $f = 2.45$ GHz, and $E_p = 300$ V/m for other frequencies. The other external conditions are the same as in Fig. 1. The dashed lines correspond to the Maxwellian EEDFs calculated at $T_{\rm eff}$ corresponding to the effective electron temperatures obtained from the more complicated numerical model (the temperatures are presented in Table II).

TABLE II. Dust charge and effective electron temperature for different rf frequencies, which were obtained from the simplified and more accurate models, and the differences between the parameters calculated using the different models. The external conditions are the same as in Fig. 2.

f (MHz)	$Z_d(-e) = Z_1$ obtained using the simplified model	$Z_d(-e) = Z_2$ obtained from the more accurate model	$\frac{\lvert Z_1 - Z_2\rvert}{Z_2} \times 100\%$	$T_{\text{eff}}(\text{eV}) = T_1$ obtained using the simplified model	$T_{\text{eff}}(\text{eV}) = T_2$ obtained from the more accurate model	$\frac{\lvert T_1 - T_2\rvert}{T_2} \times 100\%$
0	285	292	2.4	3.91	4.17	6.24
13.56	280	292	4.11	3.74	4.08	8.33
27.12	267	283	5.65	3.30	3.83	13.84
60	219	253	13.44	2.10	2.95	28.81
2.45 × 103	141	211	33.18	0.93	2.07	55.07

an increase of the number of electrons in the middle and low energy ranges (<5 eV) [see Fig. 1(a)].

The effect of increase of dust radius on the EEDF is nearly the same as for the dust density. At an increase of a_d, while the other plasma parameters are kept fixed, the number of energetic electrons in the EEDF is decreasing, and the number of electrons in the low-energy range is increasing [Fig. 1(b)].

Since the number of energetic electrons in the EEDF is decreasing with an increase of n_d and/or a_d, the electron temperature becomes smaller when the dust density and/or dust radius become larger. Meantime, we observe that the electron temperature in dusty plasma at small n_d may become larger than that in the dust-free case (the cases $n_d = 5 \times 10^6\,\text{cm}^{-3}$ and $n_d = 0$ in Table I). In our opinion, this enlargement of T_{eff} in the dusty plasma is due to an increase of the number of electrons in the middle energy range with a decrease of the number of electrons in the EEDF tail, as compared with the dust-free plasma.

With an increase of dust density, the dust charge and dust surface potential are decreasing. When the dust radius is increasing, the dust charge becomes larger, while the dust surface potential decreases.

In Fig. 1(c), the EEDF calculated using the simplified model is compared with the Maxwellian distribution for $n_d = 0$ and $n_d = 10^8\,\text{cm}^{-3}$. One can see from Fig. 1(c) that the EEDF for the dust-free case and $f_0 < 10^{-6}\,\text{eV}^{-3/2}$ differs essentially from the Maxwellian distribution. At large dust densities, the difference is smaller because of collection of electrons by dust particles.

Note that the effects of variations of n_d and a_d on the EEDF, the electron temperature, the dust charge, and the dust surface potential are similar to those obtained by other authors [1,35–38].

B. The comparison of plasma and dust particle parameters obtained from different models

In this section, we compare the EEDFs, dust charges, and effective electron temperatures calculated using the simplified model [Eqs. (8), (9), (12), and (17)] with the parameters which were obtained from Eqs. (2), (8), and (9), applying the finite-difference method [25]. The comparison was carried out for different field frequencies, electron densities, and rf field amplitudes, and for the dc case.

In Fig. 2, the electron energy distribution functions are shown for $f = 0$ (the dc case), $f = 27.12\,\text{MHz}$, $f = 60\,\text{MHz}$, and $f = 2.45\,\text{GHz}$. The dotted lines in Fig. 2 are obtained using the simplified model, while the solid lines are calculated using the finite-difference method. The dashed lines in Fig. 2 are the Maxwellian electron energy distribution functions for the electron temperatures corresponding to the solid lines.

From Figs. 2(a) and 2(b) one can recognize that for the dc case and $f = 27.12\,\text{MHz}$ the EEDFs obtained using the simplified model are very similar to those calculated using the finite-difference method. The differences in dust charges and electron temperatures obtained from the different models

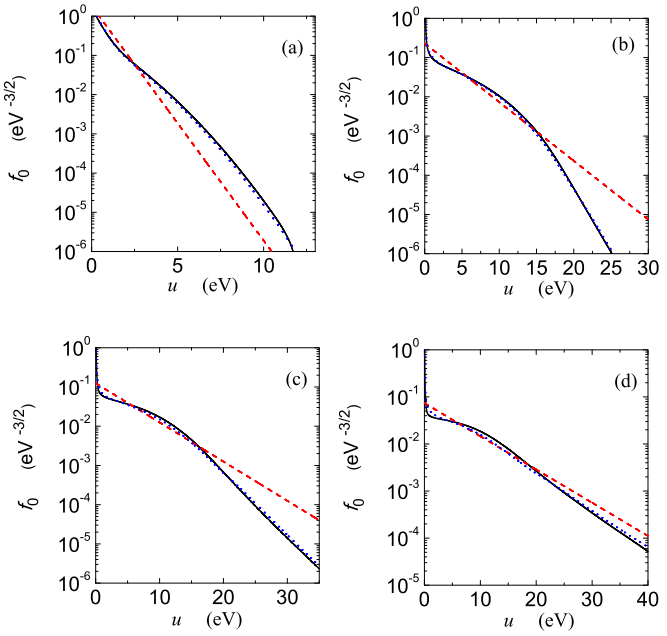

FIG. 3. (Color online) The electron energy distribution functions calculated using the simplified model (dotted lines) and the more accurate model (solid lines) for different electric field amplitudes: 100 V/m (a), 500 V/m (b), 1000 V/m (c), and 2000 V/m (d). Here, $f = 13.56\,\text{MHz}$, $n_d = 5 \times 10^7\,\text{cm}^{-3}$, $a_d = 200\,\text{nm}$, and the other external parameters are the same as in Fig. 2. The dashed lines correspond to the Maxwellian EEDFs with T_{eff} obtained from the more accurate model (Table III).

TABLE III. The same quantities as in Table II for different electric field amplitudes. The external parameters are the same as in Fig. 3.

E_p (V/m)	$Z_d(-e) = Z_1$ obtained using the simplified model	$Z_d(-e) = Z_2$ obtained from the more accurate model	$\frac{\lvert Z_1 - Z_2\rvert}{Z_2} \times 100\%$	$T_{\text{eff}}(\text{eV}) = T_1$ obtained using the simplified model	$T_{\text{eff}}(\text{eV}) = T_2$ obtained from the more accurate model	$\frac{\lvert T_1 - T_2\rvert}{T_2} \times 100\%$
100	143	148	3.38	0.68	0.73	6.06
500	278	286	2.80	2.75	2.9	5.17
1000	321	337	4.75	3.93	4.35	9.66
2000	364	385	5.45	5.5	6.15	10.57

are also small (<6% for dust charge and <14% for T_{eff}) at $f \leqslant 27.12$ MHz (Table II). However, at large rf frequencies ($f \geqslant 60$ MHz), the EEDF and dust charge calculated using the simplified model differ essentially from those obtained from Eq. (2) which take into account the electron-electron collisions and the term describing inelastic electron-atom collisions in the form of Eq. (4) [see Figs. 2(c) and 2(d)]. At $f = 60$ MHz, the difference is about 13.5% for Z_d and it is about 29% for T_{eff}.

One can conclude from Fig. 2 and Table II that the differences between the dusty plasma parameters (f_0, Z_d, and T_{eff}) obtained from the simplified model and those calculated using the more accurate model are increasing when the rf frequency becomes larger.

For low electron densities considered here ($n_e = 10^9\,\text{cm}^{-3}$), the effect of electron-electron collisions on the EEDF is small, and, therefore, the EEDF and other dusty plasma parameters obtained from the simplified model differ from those calculated using the more accurate model mainly because of neglect in Eq. (4) of the term which describes transformation of high-energetic electrons (with $u > 11.5$ eV) into low-energetic electrons by inelastic electron-atom collisions. The transformation of high-energetic electrons affects essentially the EEDF at large field frequencies due to the fact that the EEDF becomes more Maxwellian-like when the rf frequency increases [40,48]. Because of the Maxwellization, the number of energetic electrons with respect to that in the middle energy range increases, and the effect of the former term in Eq. (4) on the energy distribution becomes more important. The Maxwellization at an increase of rf frequency is accompanied by a decrease of T_{eff} and, as a result, by a decrease of dust charge (see Table II).

The effect of transformation of high-energetic electrons on the EEDF may also be essential at large electric fields E_p, when the relative number of electrons with energy $u > 11.5$ eV becomes large. To check this, we carried out our analytical calculations for different electric field amplitudes. In Fig. 3, the electron energy distribution functions are presented for $E_p = 100, 500, 1000$, and 2000 V/m.

In Table III, the dust charges and effective electron temperatures obtained using the simplified and more accurate models are shown for different electric field amplitudes.

Obviously, one can conclude from Fig. 3 and Table III that the simplified model yields results which are close to those obtained using the more accurate model, for different rf amplitudes. With increasing E_p, the difference in the EEDF slightly increases (Fig. 3). As a result, the difference in effective electron temperature also becomes larger (Table III). The difference in T_{eff} does not exceed 10.6% for the external parameters considered here, while the difference in dust charge is less than 5.5%.

Note that the EEDF at large rf field amplitudes is closer to the Maxwellian distribution than that at low E_p. In our opinion, the variation of the EEDF shape is due to increasing the number of high-energetic electrons (with $u > 11.5$ eV) at increasing E_p while simultaneously decreasing the electron's number in the energy range $e\varphi_s < u < 11.5$ eV, as compared with the dust-free case. This conclusion concerning the variation of the EEDF shape is in agreement with the results presented in Refs. [24,25].

In our simplified model, we also neglected the term describing electron-electron collisions [Eq. (7)]. However, the effect of these collisions on the EEDF increases with an increase of n_e (Fig. 4). At low electron densities ($n_e \sim$

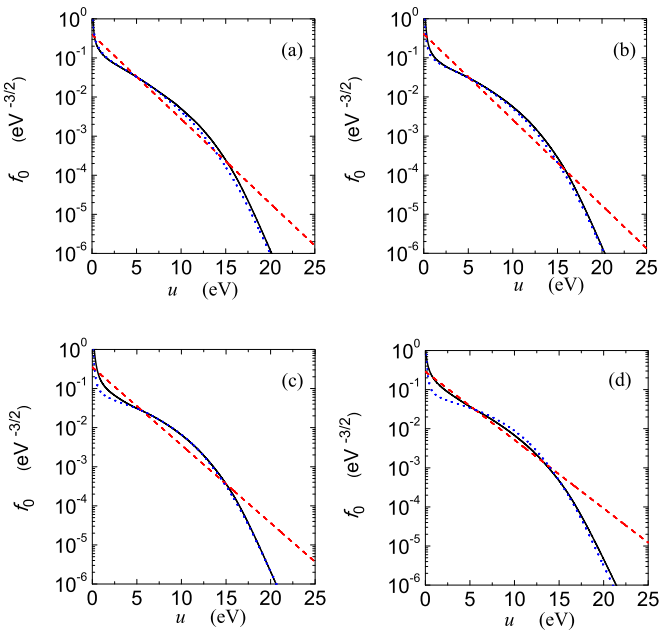

FIG. 4. (Color online) EEDFs for different electron densities: $n_e = 10^9$ (a), 10^{10} (b), 10^{11} (c), and $10^{12}\,\text{cm}^{-3}$ (d). The solid and dotted lines correspond to the EEDFs obtained using the more accurate and simplified models, respectively. Here, $E_p = 300$ V/m and the other parameters are the same as in Fig. 3. The dashed lines correspond to the Maxwellian EEDFs with T_{eff} obtained from the more accurate model (Table IV).

TABLE IV. The same quantities as in Table II for different electron densities. The external parameters are the same as in Fig. 4.

n_e (cm^{-3})	$Z_d(-e) = Z_1$ obtained using the simplified model	$Z_d(-e) = Z_2$ obtained from the more accurate model	$\frac{\lvert Z_1 - Z_2\rvert}{Z_2} \times 100\%$	$T_{\text{eff}}(\text{eV}) = T_1$ obtained using the simplified model	$T_{\text{eff}}(\text{eV}) = T_2$ obtained from the more accurate model	$\frac{\lvert T_1 - T_2\rvert}{T_2} \times 100\%$
10^9	237	244	2.87	1.91	2.01	4.98
10^{10}	470	484	2.89	1.84	1.98	7.07
10^{11}	722	724	0.28	2.0	2.18	8.26
10^{12}	889	844	5.33	2.4	2.48	3.23

$10^9\,\text{cm}^{-3}$) for $f = 13.56\,\text{MHz}$ and $E_p = 300\,\text{V/m}$, the effective electron temperature calculated from the simplified model is 4.98% smaller than that obtained applying the finite-difference method and accounting for ν_{ee} (Table IV). For $n_e \sim 10^9\,\text{cm}^{-3}$, the difference in dust charge obtained using the different approaches is 2.87%. With increasing n_e, the effective electron temperature becomes larger due to a decrease of the ratio $|n_d Z_d/n_e|$, which is accompanied by decreasing the effect of dust particles on the EEDF. When the electron density becomes larger, the difference between the EEDF obtained from the more accurate model and the Maxwellian distribution at $u < 15\,\text{eV}$ becomes smaller. This modification of the EEDF shape is due to electron-electron collisions. Since electron-electron collisions are not accounted for in the simplified model, the shape of the EEDF obtained using this model depends slightly on electron density, and the difference between the EEDF and that obtained from the more accurate model becomes larger, when n_e increases. Meantime, the difference in T_{eff} does not exceed 8.3% for the electron densities considered here, while the difference in dust charge is less than 5.4% (Table IV).

V. CONCLUSIONS

Analytical expressions (12) and (17) describing the electron energy distribution in a dusty argon plasma have been obtained. The expressions have been derived using a simplified approach, in which electron-electron collisions and transformation of high-energy electrons into electrons with low energy ($u < 11.5\,\text{eV}$) were neglected. Using this simplified model, the EEDF, effective electron temperature, dust charge, and dust surface potential have been studied for different dust densities, dust radii, field frequencies, electron densities, and amplitudes of rf field. The dusty plasma parameters have been compared with those obtained from a more accurate numerical model, in which the transformation of high-energy electrons into electrons with low energy and the electron-electron collisions were accounted for. It has been found that the simplified model can be used for calculation of the EEDF and dusty plasma parameters at typical experimental conditions, in particular, in the dc case and for an rf plasma maintained by an electric field with rather low frequency $f = 13.56\,\text{MHz}$.

Note that our approach for EEDF description at moderate energies is different from that proposed by previous authors [40,41,48], even in the dust-free case. While in the previous works it was suggested that the EEDF for dust-free plasma in the energy range $u^* < u < u^* + (3/2)T_{\text{eff}}$ could be obtained neglecting inelastic electron-atom collisions, we account for these collisions. In the dusty plasma case, we take into account the electron-atom collisions, as well as the inelastic electron-dust collisions, which are important at $u > -\varphi_s$.

Meantime, the analytical model proposed here has some limitations. Since we neglect the transformation of high-energy electrons into low-energy electrons at inelastic electron-neutral collisions, the simplified model may be inapplicable at relatively large rf frequencies ($f \geqslant 60\,\text{MHz}$), when the number of energetic electrons with respect to that in the middle-energy range can be large. The deviations between the EEDF obtained from the simplified model and that from the more accurate model become larger with increasing electron density and rf field amplitude. However, for the electron densities and rf field amplitudes considered here ($n_e \leqslant 10^{12}\,\text{cm}^{-3}$ and $E_p \leqslant 2000\,\text{V/m}$), the differences between the effective electron temperatures and dust charges obtained from the simplified and more accurate models do not exceed 11% and 5.5%, respectively (Tables III and IV). The model applicability is also limited by the validation of the local approach used here [Eq. (1)]. Therefore, the simplified model is not applicable at small plasma volumes and low neutral gas pressures. Meantime, with increasing dust density and/or dust radius the electron mean free path for momentum transfer and the energy relaxation length become smaller, and the local approach, inapplicable for a dust-free plasma case, may become applicable for consideration of dusty plasma.

Using Eqs. (12) and (17), one can find more easily the electron energy distribution function in a dusty plasma, as compared with other approaches usually used for the EEDF calculation (finite-difference methods, particle-in-cell–Monte Carlo models, and hybrid models). The approach used here can also be applied for obtaining the EEDF in other plasma systems, including but not limited to those used for the fabrication of nano- and microsized structures.

ACKNOWLEDGMENT

This work was supported by the State Fund for Fundamental Research of Ukraine.

[1] *Dusty Plasmas: Physics, Chemistry, and Technological Impacts in Plasma Processing*, edited by A. Bouchoule (Wiley, New York, 1999).

[2] S. V. Vladimirov and K. Ostrikov, Phys. Rep. **393**, 175 (2004).

[3] V. E. Fortov, A. V. Ivlev, S. A. Khrapak, A. G. Khrapak, and G. E. Morfill, Phys. Rep. **421**, 1 (2005).

[4] P. K. Shukla and B. Eliasson, Rev. Mod. Phys. **81**, 25 (2009).

[5] H. Kersten, H. Deutsch, E. Stoffels, W. W. Stoffels, G. M. W. Kroesen, and R. Hippler, Contrib. Plasma Phys. **41**, 598 (2001).

[6] L. Boufendi and A. Bouchoule, Plasma Sources Sci. Technol. **11**, A211 (2002), and the references therein.

[7] E. Stoffels, W. W. Stoffels, H. Kersten, G. H. P. M. Swinkels, and G. M. W. Kroesen, Phys. Scr. T **89**, 168 (2001).

[8] M. Mikikian and L. Boufendi, Phys. Plasmas **11**, 3733 (2004).

[9] U. Kortshagen and U. Bhandarkar, Phys. Rev. E **60**, 887 (1999).

[10] E. Kovacevic, I. Stefanovic, J. Berndt, Y. J. Pendleton, and J. Winter, Astrophys. J. **623**, 242 (2005).

[11] F. X. Bronold, H. Fehske, H. Kersten, and H. Deutsch, Phys. Rev. Lett. **101**, 175002 (2008).

[12] F. X. Bronold, H. Fehske, H. Kersten, and H. Deutsch, Contrib. Plasma Phys. **49**, 303 (2009).

[13] O. Arp, D. Block, A. Piel, and A. Melzer, Phys. Rev. Lett. **93**, 165004 (2004).

[14] H. Thomas, G. E. Morfill, V. Demmel, J. Goree, B. Feuerbacher, and D. Möhlmann, Phys. Rev. Lett. **73**, 652 (1994).

[15] V. I. Kolobov and V. A. Godyak, IEEE Trans. Plasma Sci. **23**, 503 (1995).

[16] U. Kortshagen, C. Busch, and L. D. Tsendin, Plasma Sources Sci. Technol. **5**, 1 (1996).

[17] M. A. Lieberman and A. J. Lichtenberg, *Principles of Plasma Discharges and Materials Processing* (Wiley, New York, 2005).

[18] S. K. Nam and J. P. Verboncoeur, Comput. Phys. Commun. **180**, 628 (2009).

[19] T. Misawa, S. Nunomura, N. Ohno, and S. Takamura, Jpn. J. Appl. Phys. **39**, L551 (2000).

[20] N. Bilik, R. Anthony, B. A. Merritt, E. S. Aydil, and U. R. Kortshagen, J. Phys. D **48**, 105204 (2015).

[21] B. Layden, V. Cheung, and A. A. Samarian, IEEE Trans. Plasma Sci. **39**, 2762 (2011).

[22] A. Bouchoule and L. Boufendi, Plasma Sources Sci. Technol. **3**, 292 (1994).

[23] I. Denysenko, J. Berndt, E. Kovacevic, I. Stefanovic, V. Selenin, and J. Winter, Phys. Plasmas **13**, 073507 (2006).

[24] M. K. Deka, H. Bailung, and N. C. Adhikary, Chin. Phys. B **22**, 045201 (2013).

[25] I. Denysenko, M. Y. Yu, K. Ostrikov, N. A. Azarenkov, and L. Stenflo, Phys. Plasmas **11**, 4959 (2004).

[26] D. Samsonov and J. Goree, Phys. Rev. E **59**, 1047 (1999); IEEE Trans. Plasma Sci. **27**, 76 (1999).

[27] I. Denysenko, K. Ostrikov, M. Y. Yu, and N. A. Azarenkov, Phys. Rev. E **74**, 036402 (2006).

[28] M. J. McCaughey and M. J. Kushner, J. Appl. Phys. **69**, 6952 (1991).

[29] J. P. Boeuf, Phys. Rev. A **46**, 7910 (1992).

[30] I. V. Schweigert, A. L. Alexandrov, and D. A. Ariskin, Plasma Chem. Plasma Process. **34**, 671 (2014).

[31] W. J. Goedheer, M. R. Akdim, and Yu. I. Chutov, Contrib. Plasma Phys. **44**, 395 (2004).

[32] A. L. Alexandrov, I. V. Schweigert, and F. M. Peeters, New J. Phys. **10**, 093025 (2008).

[33] G. I. Sukhinin and A. V. Fedoseev, Phys. Rev. E **81**, 016402 (2010).

[34] G. I. Sukhinin, A. V. Fedoseev, T. S. Ramazanov, R. Zh. Amangaliyeva, M. K. Dosbalayev, and A. N. Jumabekov, J. Phys. D **41**, 245207 (2008).

[35] D. Wang and J. Q. Dong, J. Appl. Phys. **81**, 38 (1997).

[36] I. Denysenko, M. Y. Yu, and S. Xu, J. Phys. D **38**, 403 (2005).

[37] I. Denysenko, M. Y. Yu, K. Ostrikov, and A. Smolyakov, Phys. Rev. E **70**, 046403 (2004).

[38] K. Ostrikov, I. Denysenko, M. Y. Yu, and S. Xu, J. Plasma Phys. **71**, 217 (2005).

[39] I. P. Shkarofsky, T. W. Johnston, and M. P. Bachynski, *The Particle Kinetics of Plasmas* (Addison-Wesley, Reading, MA, 1966).

[40] L. M. Biberman, V. S. Vorobev, and I. T. Yakubov, *Kinetics of Nonequilibrium Low-Temperature Plasma* (in Russian) (Moscow, Nauka, 1982).

[41] B. M. Smirnov, *Physics of Weakly Ionized Gas in Problems with Solutions* (in Russian) (Moscow, Nauka, 1985).

[42] R. Winkler, J. Wilhelm, and A. Hess, Ann. Phys. (Leipzig) **497**, 537 (1985).

[43] R. Winkler, M. Capitelli, M. Dilonardo, C. Gorse, and J. Wilhelm, Plasma Chem. Plasma Process. **6**, 437 (1986).

[44] C. M. Ferreira and J. Loureiro, Plasma Sources Sci. Technol. **9**, 528 (2000)

[45] W. Lochte-Holtgreven, *Plasma Diagnostics* (North-Holland, Amsterdam, 1968), p. 675.

[46] S. A. Khrapak, S. V. Ratynskaia, A. V. Zobnin, A. D. Usachev, V. V. Yaroshenko, M. H. Thoma, M. Kretschmer, H. Hofner, G. E. Morfill, O. F. Petrov, and V. E. Fortov, Phys. Rev. E **72**, 016406 (2005).

[47] A. V. Phelps and Z. Lj. Petrovic, Plasma Sources Sci. Technol. **8**, R21 (1999).

[48] V. E. Golant, A. P. Zhilinskii, and I. E. Sakharov, *Fundamentals of Plasma Physics* (Wiley, New York, 1980).